LIQUEFACTION AT THE IMPERIAL VALLEY WILDLIFE SITE

R.O. Davis[1] and J.B. Berrill[2]

ABSTRACT

In November 1987, two earthquakes occurred near a site in the Imperial Valley, California, where extensive field instrumentation had been placed by the US Geological Survey. The site was part of a wildlife refuge and has come to be called the Wildlife Site, or simply Wildlife. Some controversy arose subsequent to the earthquakes because of concern the field piezometers at the site may not have responded accurately in the second, larger earthquake. In this paper we re-examine the data from both earthquakes in an effort to (i) better understand the response of Wildlife during shaking, (ii) shed some light on the validity of the measured pore pressures from the larger earthquake, and (iii) investigate an alternative hypothesis for how liquefaction may develop.

INTRODUCTION

The Wildlife Site became of interest following the Westmorland earthquake in 1981. That earthquake appeared to have caused liquefaction in certain areas, Wildlife being one. The site was subsequently instrumented with two accelerometers, one at –7.5 m depth below ground surface and one at ground surface; and with six piezometers at depths ranging between –2.9 m and -12.0 m. Site stratigraphy is illustrated in Figure 1. A layer of silt approximately 2.5 m thick overlies a 4.5 m thick layer of silty sand. The silty sand was presumed to be the liquefiable soil at the site. It lay above a 5 m thick layer of stiff clay. Of the six piezometers, five were placed in the silty sand layer. The ground water table was located at a depth of approximately 1.2 m. The downhole accelerometer was positioned near the upper surface of the stiff clay.

In November 1987, two earthquakes occurred near Wildlife within a period of 12 hours. The first was the Elmore Ranch earthquake. It had magnitude 6.2 and was located approximately 23 km west from Wildlife. The second was the Superstition Hills earthquake, magnitude 6.6, located approximately 31 km to the west and south from Wildlife. At the ground surface the peak measured acceleration for the Elmore Ranch event was 0.13g, and for the Superstition Hills event, 0.21g. None of the field piezometers indicated significant pore pressure increase for the Elmore Ranch event, but four piezometers located in the silty sand layer recorded large pore pressure changes for the Superstition Hills event. One other piezometer in the silty sand did not operate properly and the sixth piezometer was located in deeper soil below the liquefying layer.

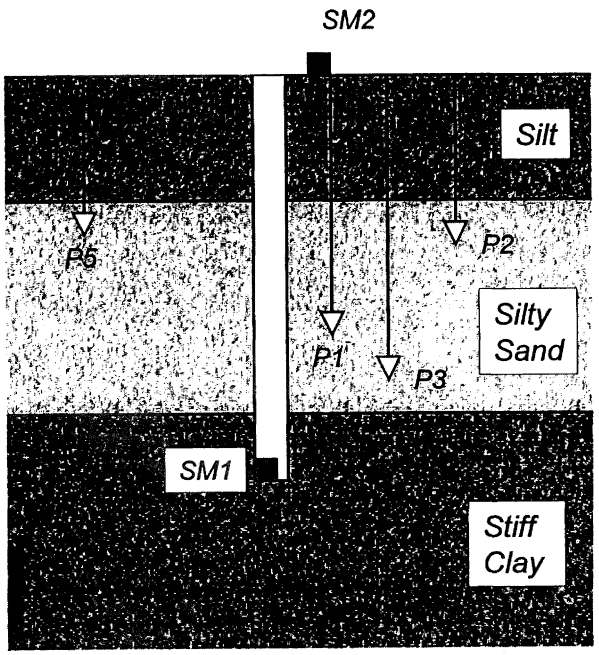

Figure 1. Schematic soil profile at Wildlife. Downhole and Surface accelerometers denoted by square boxes SM1 and SM2. Piezometers are denoted by triangles P1, P2, P3 and P5. Piezometers P4 and P6 are not relevant to this study.

Holzer, *et al.* (1989), reported on the measured pore pressures from the Superstition Hills event. They suggested the silty sand layer had liquefied during the earthquake. Their suggestion was based on both the recorded pore pressures and on surface evidence of sand boils and lateral spreading features. Subsequently questions were raised concerning the unexpectedly long rise times recorded by the pore pressure transducers. When compared with the duration of strong ground shaking, it appeared to some analysts that the measured pore pressure response was considerably slower than seemed reasonable. Because of this, Hushmand, *et al.* (1992) attempted to recalibrate the field piezometers *in situ*.

[1] *Department of Civil Engineering, University of Canterbury, New Zealand (Member).*
[2] *Department of Civil Engineering, University of Canterbury, New Zealand (Fellow).*

They tested each of the existing piezometers by inserting a new piezometer close by and then artificially generating a pore pressure pulse in the ground. They then compared the readings of the existing and newly inserted piezometers. The comparisons revealed that the response of the existing piezometers was similar to that for the newly inserted instrument in only one case. Hushmand, *et al.* (1992) did not suggest liquefaction might not have occurred. Indeed everyone seems to agree liquefaction did occur. They did suggest, however, that the pore pressure response rise times might be too slow.

Subsequent to the recalibration experiments by Hushmand, *et al.* (1992), Youd and Holzer (1994) defended the original pore pressure recordings. They noted how interbedding of silt and sand at the site might possibly affect the response of two piezometers separated by small but significant distances. They also noted how the ground motion at the site continued for many seconds beyond the period of strong shaking and how this motion may have contributed to pore pressure generation. For further corroboration they cited the analysis by Zeghal and Elgamal (1994) in which the measured accelerations were used to estimate the shear stress-strain time history within the upper most 7.5 m of soil. Zeghal and Elgamal's analysis showed that softening of the site soils continued to occur beyond the period of strong shaking.

The Wildlife records remain a unique resource in the field of earthquake geotechnical engineering. While the fidelity of the pore pressure recordings can never be guaranteed with complete confidence, the arguments from both sides of the issue are persuasive. If one does accept the records as accurate, then it must also be accepted that our conventional knowledge of how liquefaction occurs may be flawed. The records suggest that once pore pressures begin to rise, even quite low levels of shaking may lead to further gradual increases. If, on the other hand, the piezometers did not respond accurately, questions arise regarding the nature of the inaccuracies and whether any of the data can be salvaged. Between the two extremes is the possibility that some of the records were accurate while others were inaccurate.

One thing is certain, the Elmore Ranch earthquake caused no pore pressure increase, but the Superstition Hills earthquake caused complete liquefaction. The major difference between the two events was a very brief period of stronger shaking in the Superstition Hills earthquake. That brief period may have acted as a trigger, setting the pore pressure rise mechanism in motion. Subsequent lesser ground shaking, similar to the Elmore Ranch earthquake, then continued to induce greater pore pressure until liquefaction resulted. The idea of a trigger or critical value of shaking is quite similar to the threshold shear strain theory of Dobry *et al.* (1982). They suggested a critical strain value exists for which large scale grain rearrangement will commence. For smaller strain levels, the intergranular contacts would remain elastic or elastic-plastic, but complete slip would not occur. At the threshold strain, the entire contact slips and the grains begin to displace relative to one another. Only minor pore pressure changes can occur prior to the threshold strain. Once the threshold is reached, large pore pressure increases may occur.

In this paper, we re-examine the Wildlife records using a collection of ideas. Initially we will model the softening of the upper 7.5 m of the site using a technique devised by Davis (2000) that correlates the downhole and surface acceleration records using a time compression algorithm. We will show that the apparent softening commenced at roughly the time pore pressures began to rise and continued somewhat beyond the period of strong shaking. We will then approximate the time histories of shear stress and strain in the soil using the method of Davis and Berrill (1998). We can directly compare the average shear strain at the moment when large pore pressure changes begin with the theoretical value suggested by Dobry *et al.* (1982). Following this we will use the approximated stress and strain records to calculate the dissipated energy density in the site soils. We can then employ the widely used hypothesis that pore pressure increase depends on dissipated energy density to approximate the time history of pore pressure rise at the site. The calculated pore pressures will be compared with the measured values. These calculations will suggest two of the piezometers probably responded accurately while two others probably did not.

SOFTENING OF THE WILDLIFE SITE

If the level of shaking during an earthquake is relatively low and the site response remains elastic or nearly so, an investigator can easily determine the average soil shear modulus between two instruments in a downhole array by cross correlating two measured acceleration records. The lag time associated with the correlation peak represents the travel time between the two instruments. Dividing the vertical separation between the instruments by the travel time gives the shear wave velocity, c_S, and this immediately leads to the shear modulus, $G = \rho c_S^2$. Here ρ represents the mass density of the soil.

The interpretation of downhole array data becomes more complicated whenever significant amounts of softening occur within the soil layers as the earthquake shaking progresses. Travel time between the two instruments changes during shaking and normal cross correlation will lead only to some value of shear modulus intermediate between the initial elastic value at the onset of shaking and the final softened value when shaking stops. Recently Davis (2000) suggested a time compression algorithm to correct for softening and to create a continuous picture of the shear wave velocity between two instruments as shaking progresses. The algorithm revolves around the idea that softening retards the wave velocity. Wave arrivals at the upper instrument occur at later and later travel times. The algorithm adjusts the time scale of the upper recording in such a way that the effects of softening are compensated for. When calculations are complete, the time scale of the record from the upper instrument will have been compressed in such a way that the effects of softening have been completely removed. The new compressed record is what would have been obtained had elastic behaviour prevailed.

Figures 2(a) and 2(b) show the measured accelerations from the Superstition Hills event at Wildlife. This data was downloaded directly from the University of California at Santa Barbara Strong Motion Database. The peak horizontal acceleration at the ground surface was 0.21g in the North-South record at roughly 13.6s after triggering. The peak acceleration at the –7.5 m depth was 0.17g, also in the North-South record at roughly the same time. Even a cursory inspection of the records suggests that significant softening occurred following the peak values. A lower predominant

frequency is evident, as are the characteristic acceleration spikes separated by more or less flat response at the ground surface. These acceleration spikes have been implicated in a number of earthquakes as evidence of softening, probably due to liquefaction (Archuleta, 1998).

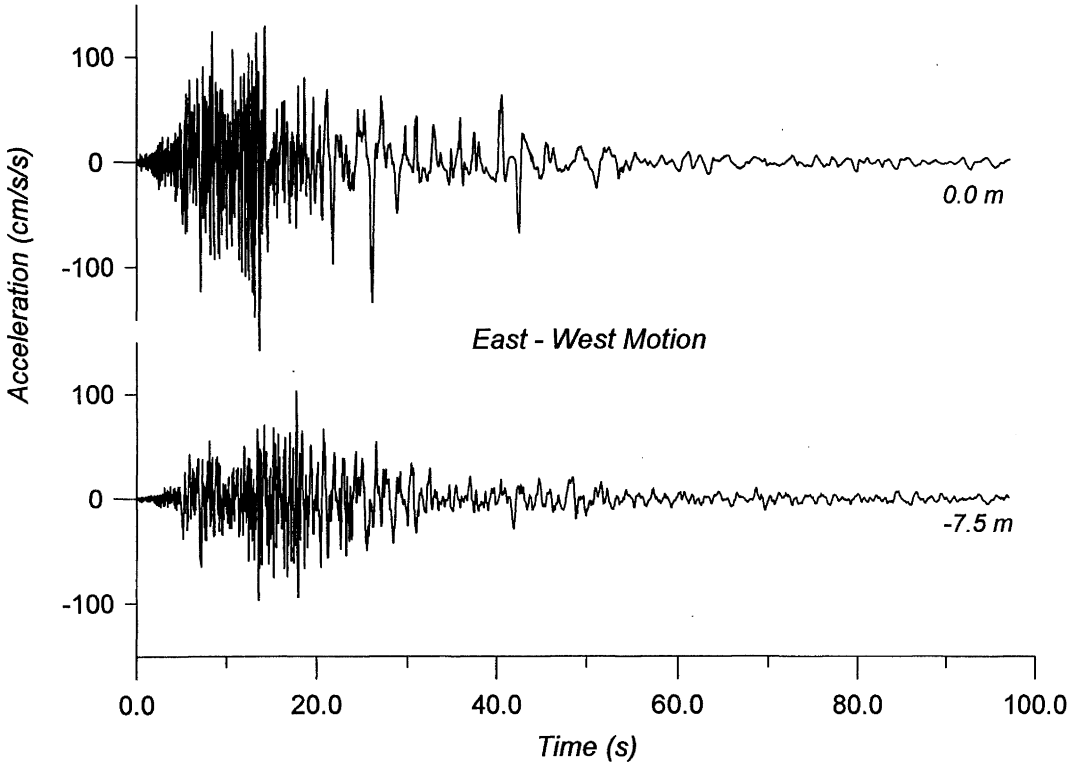

Figure 2 (a). Measured accelerations from Superstition Hills earthquake: East-West data.

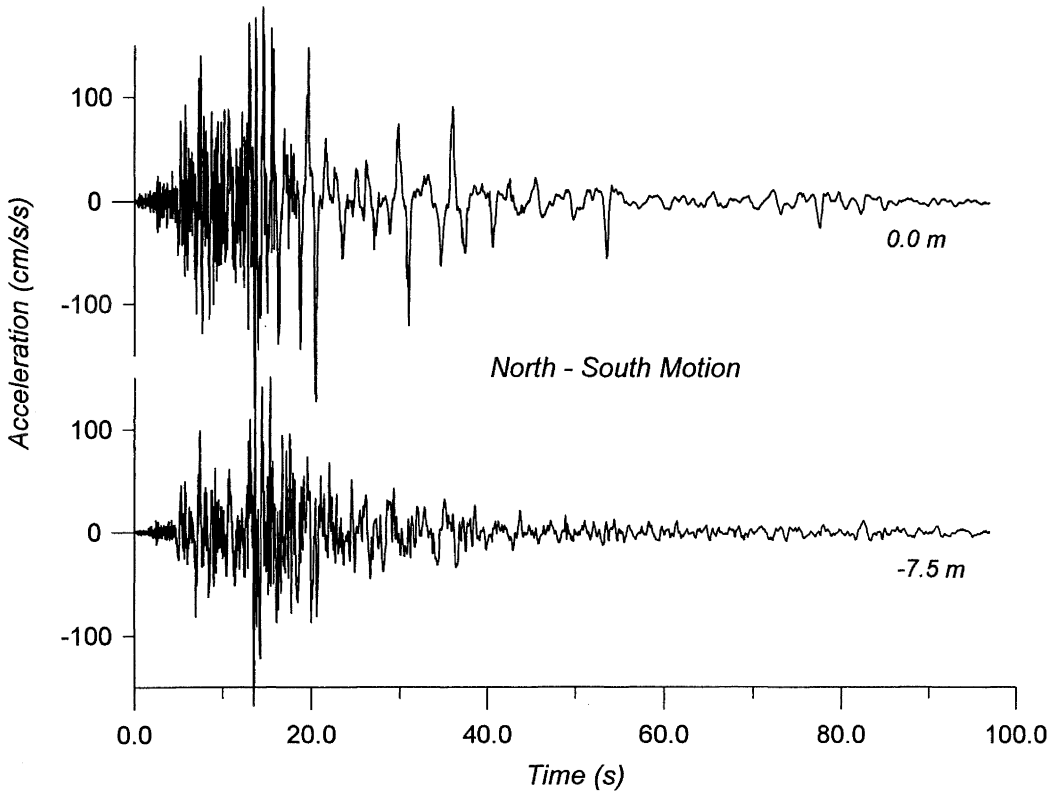

Figure 2 (b). Measured accelerations from Superstition Hills earthquake: North-South data.

Both the East-West and North-South records were analysed using the time compression algorithm (Davis, 2000). For the East-West record, the lag time corresponding to the peak correlation after time compression was found to be 0.06s. This value is the travel time τ_o between the two instruments for elastic waves. If we let c_{so} represent the initial, elastic shear wave velocity for Wildlife, then the East-West record suggests $c_{so} = 7.5\ m/\tau_o = 125\ m/s$. This value coincides exactly with the wave velocity cited by Holzer *et al.* (1989). For the North-South record, the time compression algorithm suggested a value for τ_o of 0.075s, corresponding to an elastic shear wave speed of 100 m/s. It is felt the East-West value is more reliable than the North-South.

Next, let Δ denote the cumulative time compression for the upper acceleration record at time *t*. That is, Δ is the total amount by which the upper acceleration time scale must be compressed, up to the time *t*, in order to overcome the effects of softening. Then the average shear wave velocity for the site at that time is given by

$$c_s = \frac{7.5\,m}{\tau_o + \Delta} \qquad (1)$$

Graphs of Δ for both North-South and East-West records are shown in Figure 3. Note that increasing values of Δ imply decreasing shear wave velocity. Significant softening begins sometime between 13 to 14 seconds. Quite large cumulative time compressions are found for both records. The time compression is roughly the same up to about 40 seconds. After this point the two records begin to differ. The North-South record exhibits a decrease followed by a large increase reaching values in excess of 1.5s. The East-West record shows a more subdued response, increasing gradually to a value of about 0.8s. It should be noted that the time compression algorithm involves a large number of optimisations and, as is the case in any complex optimisation problem, spurious results may arise. We suggest that the later behaviour in the North-South record may not be representative of the true ground response. Recalling that the East-West response gave the best estimate for the elastic wave velocity, it seems likely the overall time compression behaviour will be more representative than the North-South data.

Graphs of shear wave velocity calculated using equation (1) with $\tau_o = 0.06\ s$ are shown in Figure 4. As in Figure 3, the solid line corresponds to the East-West motion, the dashed line to the North-South. It is helpful to consider three separate segments of this figure.

First, between zero and roughly 13 seconds, the behaviour of c_s appears jagged and erratic. This occurs despite small variations in Δ (as can be clearly seen from the comparable time interval on Figure 3). In fact the small Δ variations result in greatly magnified changes in c_s. Note from equation (1) that a change as small as 0.005s (the digitisation interval for the Wildlife accelerograms) in Δ will result in a change of shear wave velocity of nearly ten percent. It is clear that early in the record, when the soil is elastic, the approximation of c_s is extremely sensitive to minor variations in time compression. Because of this the jagged response is not considered representative of the real soil.

Second, between 13 and roughly 20 seconds, c_s decreases dramatically. This corresponds to the rapid rise in time compression seen on Figure 4. Both the East-West and North-South records appear to respond in a nearly identical way. This time interval also contains the strongest accelerations.

Finally, from about 17 seconds to the end of the record, the c_s behaviour appears to be relatively flat. The East-West and North-South data agree fairly well, although the North-South response gives a slightly greater c_s between 40 and 60 seconds.

It is useful to compare Figures 3 and 4 in terms of the overall picture of softening they present. Recalling that the value of time compression in Figure 3 is simply the amount of addition travel time due to softening that must be added to the elastic wave travel time, we see that very little change happens in the time interval between zero and 13 seconds. For the interval from 13 to 20 seconds, some change to the travel time occurs. And for the interval from 20 seconds to about 50 seconds, significant additional change, particularly for the East-West record, occurs. This is in contrast to the picture presented by Figure 4. There, erratic variations in c_s occur between zero and 13 seconds, a large decrease occurs between 13 and 20 seconds, and very little softening appears to occur following 20 seconds. Arguably, Figure 3 presents a more useful picture of softening, particularly in cases where liquefaction, and hence large amounts of softening may have occurred. We conclude from the data presented here that softening of the Wildlife soils probably persisted throughout the interval between 13 and 50 seconds. This conclusion supports the similar suggestion by Zeghal and Elgamal (1994).

Before concluding this section it is interesting to see the result of the time compression algorithm applied to the Elmore Ranch earthquake. Figure 5 shows the acceleration records for this earthquake. It preceded the Superstition Hills event by about 12 hours. Note that the acceleration axes in Figure 5 have the same scale as in Figure 2 to assist in comparing the two earthquakes. For the Elmore Ranch event the peak ground surface acceleration was slightly less than 0.13g found in both the North-South and East-West records at about 7 seconds. Comparison of Figures 2 and 5 makes clear the Elmore Ranch ground motion was not so strong as that for Superstition Hills. In particular the characteristic acceleration spikes seen later in the Superstition Hills record are absent from the Elmore Ranch record. Also, no surface features indicating liquefaction were observed following the Elmore Ranch event. One might therefore expect little softening and hence little time compression to be evident from applying the algorithm to the Elmore Ranch data.

In both the North-South and East-West cases, the time compression algorithm suggested a value of 0.07s for the elastic wave travel time τ_o. Figure 6 shows plots of the

cumulative time compression for the Elmore Ranch records. The results for both North-South and East-West records are consistent, but are also surprising. For both records, some initial small amounts of time compression are evident during the first 7 to 8 seconds, but this is followed by an apparent stiffening, corresponding to negative time compression, through to the end of the record. It is highly unlikely that actual stiffening of the site soils occurred during the later stages of this earthquake. Instead, a likely explanation is that surface waves were the predominant form of motion later in the record. The time compression algorithm assumes all the ground motion results from vertically propagating SH waves. If in fact surface waves predominate, little vertical propagation is occurring and the apparent travel time between the downhole and surface instruments is zero. The time compression algorithm apparently recognises the decreasing travel time and attempts to compensate by stretching rather than compressing the time axis for the upper record.

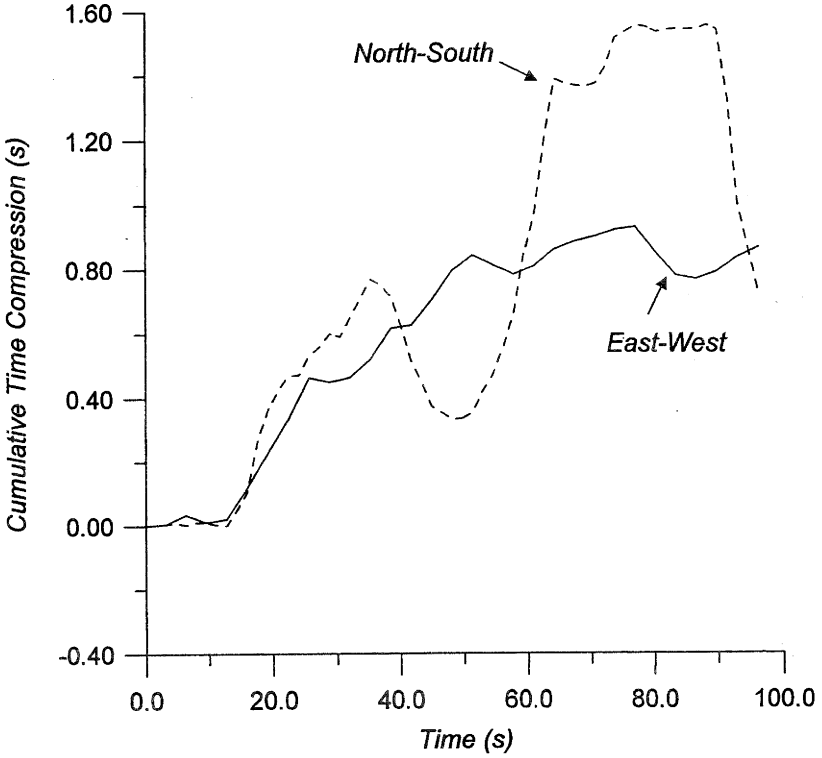

Figure 3. Cumulative time compression for Superstition Hills earthquake. The graphs represent the amount of additional travel time for waves to propagate to the surface caused by softening.

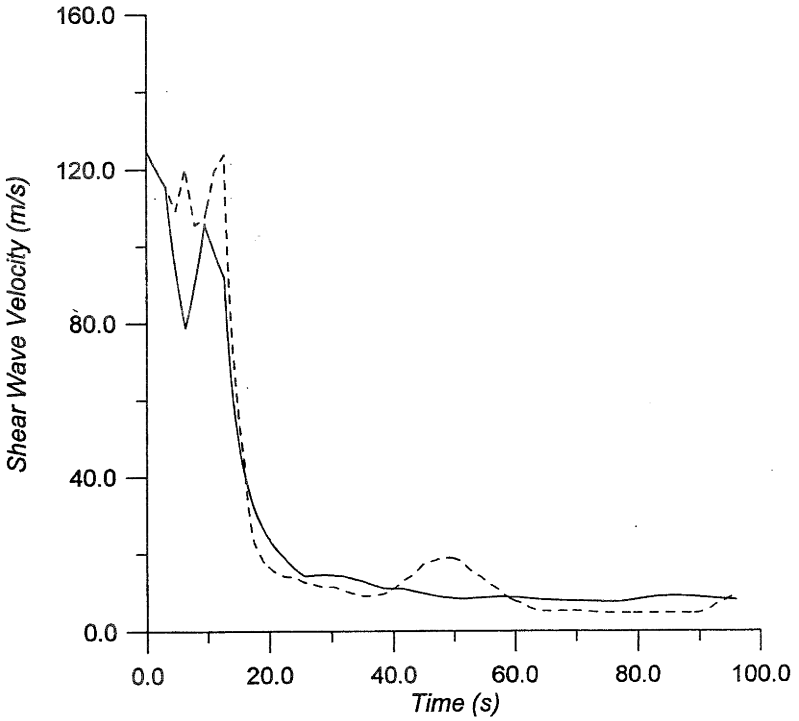

Figure 4. Shear wave velocity softening during the Superstition Hills earthquake.

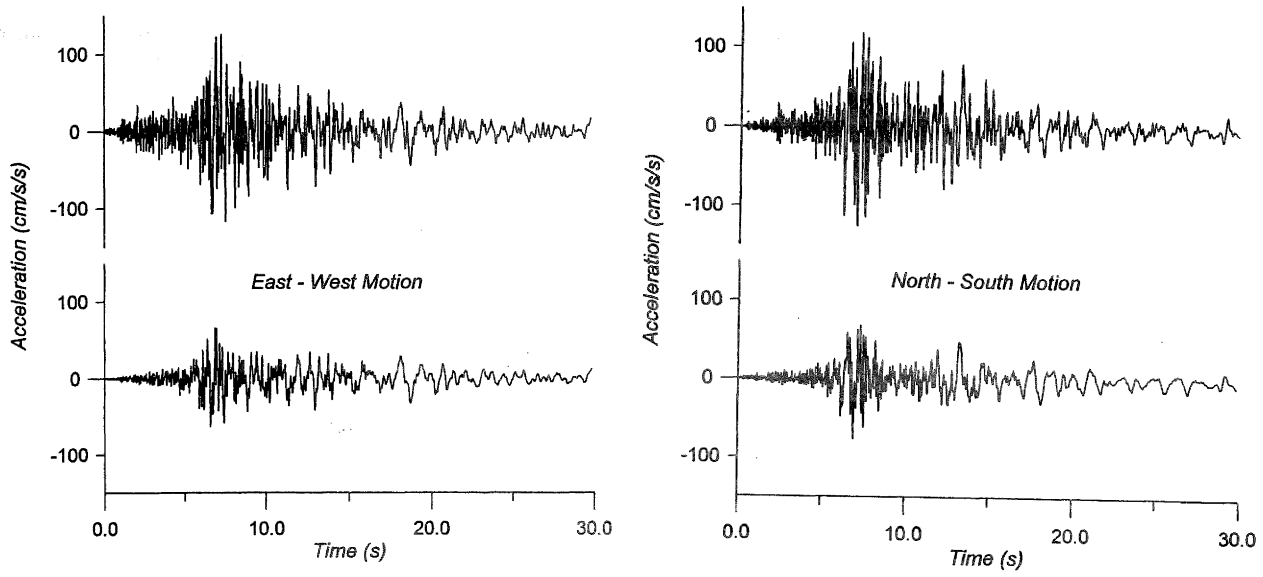

Figure 5. Measured accelerations from Elmore Ranch earthquake: (a) East-West data, (b) North-South data.

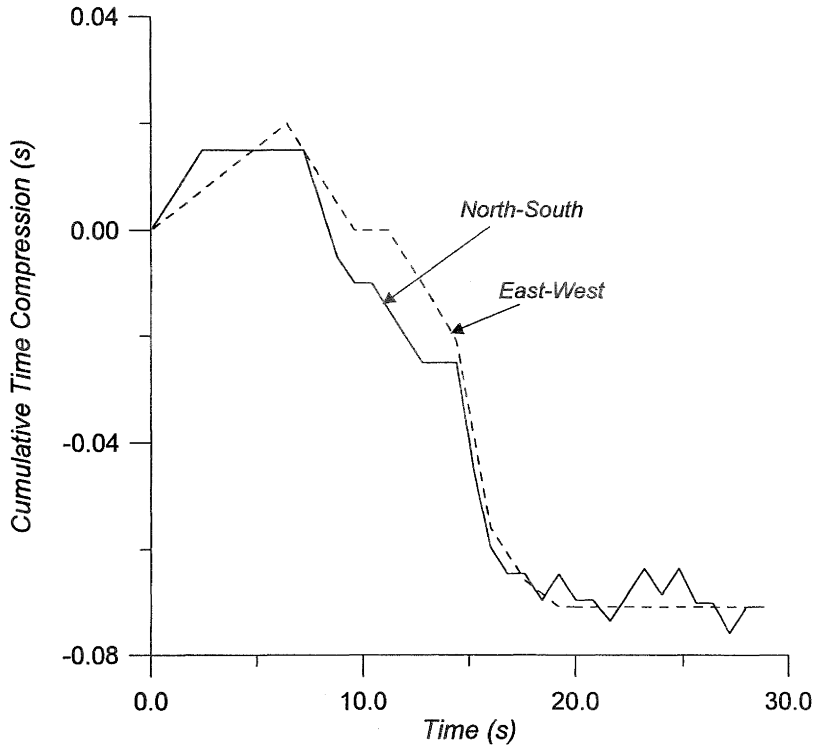

Figure 6. Cumulative time compression for Elmore Ranch earthquake. The apparent time stretching is thought to be caused by surface waves.

STRESS-STRAIN RESPONSE

The large scale softening evident in the Superstition Hills earthquake is clearly represented in the stress-strain response of the site soils. We will synthesize the shear stress and shear strain time histories at a particular depth using the analysis of Davis and Berrill (1998). A similar analysis was carried out by Zeghal and Elgamal (1994). Their analysis differs from ours in two respects. Our analysis employs approximating functions for displacement and acceleration that are sums of harmonic functions that will obey the free surface boundary condition and remain bounded for all depths. Also our analysis can take account of layered sites. Zeghal and Elgamal's analysis was more simplified, assuming homogeneous soil conditions and linear approximating functions. Nevertheless the results from their study and our own are similar.

We will consider the shear stress and strain for the Superstition Hills earthquake at one particular depth -5.0 m. This is one of the depths where piezometers were located. Later the synthesized stress-strain response will be integrated to obtain the dissipated energy density for all piezometer depths. All of the results shown in this section were obtained using the acceleration data exactly as obtained from the UCSB Strong Motion Database.

Beginning with the assumption of a homogeneous soil profile, time histories of synthesized shear stress and shear strain for the North-South motion at the -5.0 m depth are shown in Figure 7. Quite large strains develop following about 13 seconds. The peak shear strain value of 2 percent occurs at about 36 seconds and large strains persist to the end of the record despite the shear stress being small. Similar strain response is found for the East-West record.

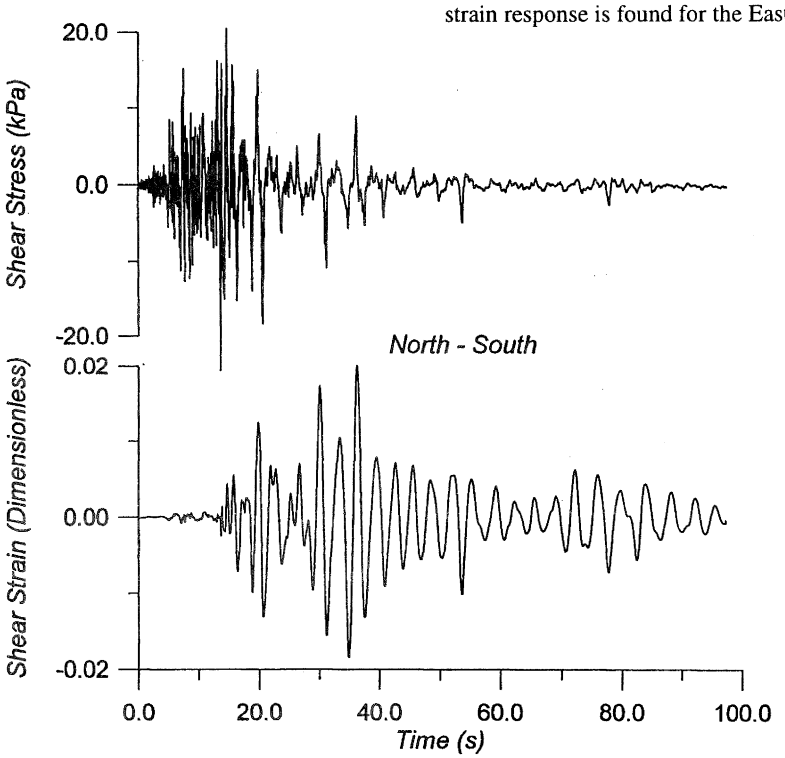

Figure 7. Synthesized shear stress and strain time histories for the Superstition Hills earthquake. Calculation at –5.0 m depth using North-South accelerations and displacements.

We can recalculate the stress-strain response using a layered soil profile by slightly modifying the analysis of Davis and Berrill (1998). In that analysis it was assumed the impedance ratio of adjacent layers remained constant. That assumption is clearly not appropriate here since liquefaction is developing in one layer. We have adapted the Davis and Berrill analysis by adjusting the shear wave velocity within the softening layer to the value suggested by the time compression analysis for the East-West data shown in Figure 4. The wave velocity in the soils above and below is held constant at 125 m/s. While the synthesized stresses are similar to those found for the homogeneous case, the computed strains are somewhat larger. This is illustrated in Figure 8 where similar segments of the strain time histories are compared.

Graphs of shear stress versus shear strain for the North-South record at the –5.0 m depth are shown in Figure 9. These were obtained using the layered analysis. The four parts of the figure illustrate the response for various time segments within the record. All have the same stress and strain scales. The earliest segment, from 13 to 18 seconds, contains the onset of large strains and the beginning stages of softening. The second segment, from 18 to 30 seconds, covers that part of the record where the majority of softening occurs. The typical banana-shaped stress-strain response for a yielding soil is clearly evident in this segment. The third segment, from 30 to 60 seconds, covers the transition from relatively strong accelerations to quite modest acceleration values. Some further softening is evident. The hysteresis loops gradually lose the banana shape in this segment. The final segment takes the time to near the end of the record and shows the extreme softening that has occurred prior to 60 seconds. Little additional softening is evident in the final 30 seconds.

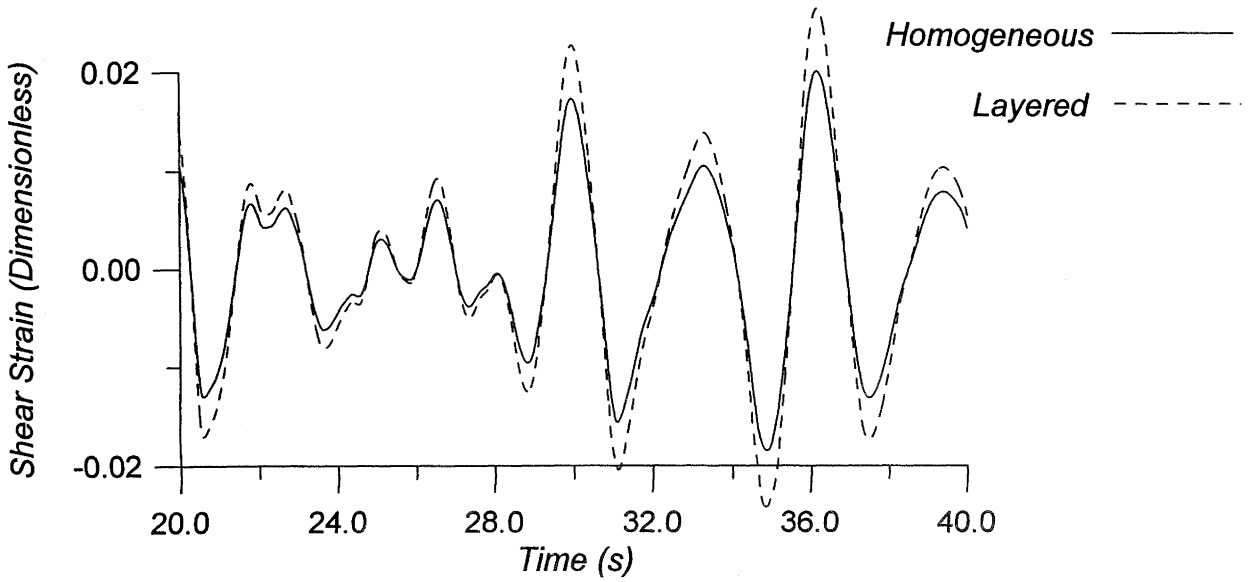

Figure 8. Comparison of synthesized strains using homogeneous and layered models.

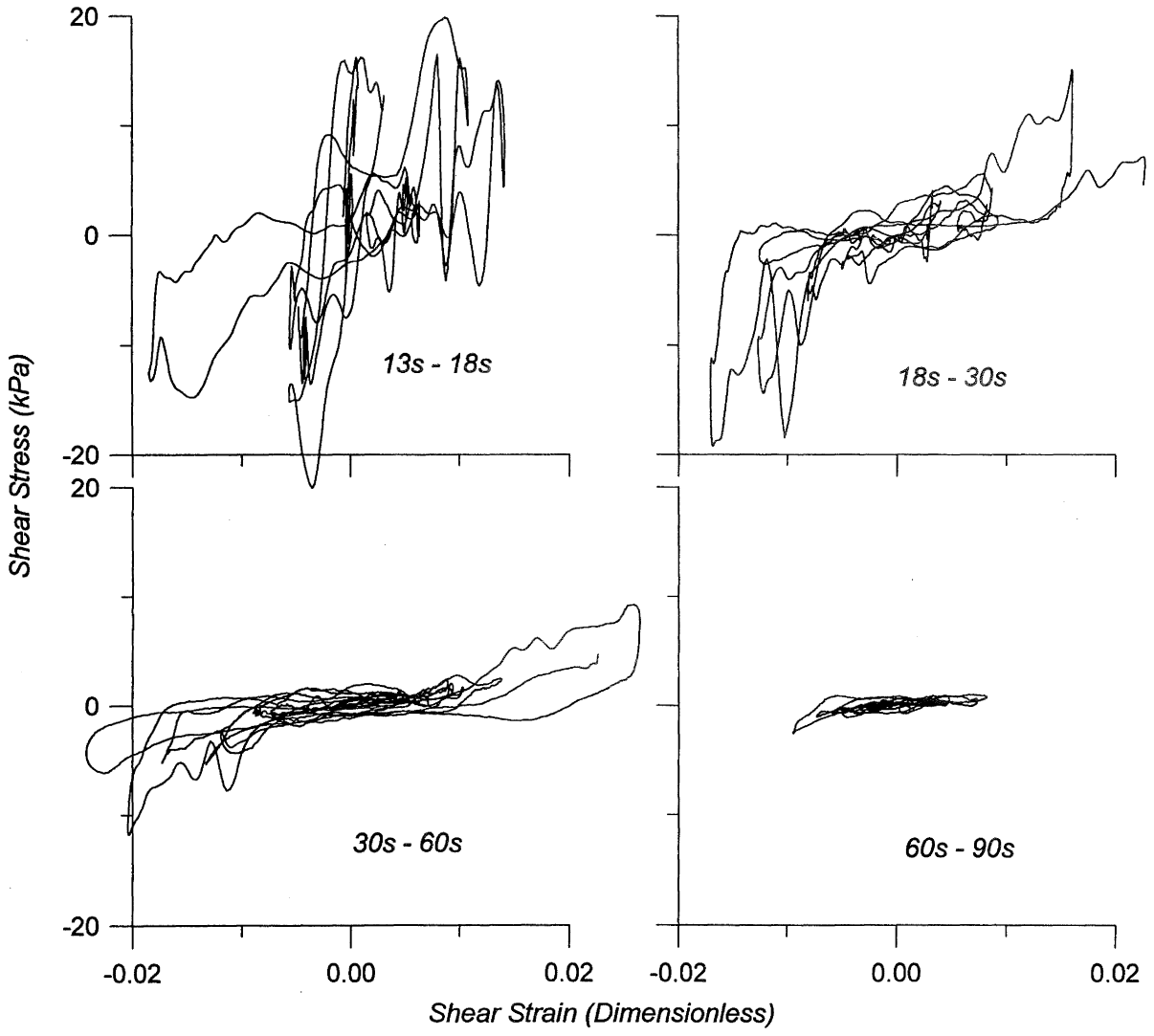

Figure 9. Synthesized stress-stress strain response from Superstition Hills earthquake. Calculation at –5.0 m depth using North-South accelerations and displacements.

It is difficult to assess the value of the soil shear modulus from plots such as those in Figure 9. As an example consider the small segment of stress strain response shown in Figure 10. The slightly jagged line on this figure is the synthesized stress versus strain behaviour for the time interval 70 to 75 seconds, a part of the lower right graph from Figure 9. Two straight lines have been plotted on the graph corresponding to two possible values for shear modulus. The solid line corresponds to a value for G of 122 kPa which is consistent with a shear wave velocity of about 7.8 m/s. This is the shear wave velocity suggested by the time compression analysis of the East-West data from Figures 3 and 4. The dashed line corresponds to a value of shear modulus of 46 kPa consistent with a shear wave velocity of about 4.8 m/s, the value suggested by the North-South data in the time compression algorithm. It would appear from the figure that the synthesized stress-strain data prefer neither one nor the other of the two possible shear moduli. We should add that the situation presented is not unusual. For nearly any time interval one may choose over the final 40 to 50 seconds of the record, the data show a similar response. The stress-strain response is organised, but only in a vague way. To attempt to draw any firm conclusions concerning the instantaneous shear modulus is nearly impossible.

The data shown here may be compared with that given by Zeghal and Elgamal (1994). In general the overall character of the stress-strain response is the same for both studies. Some minor differences occur because Zeghal and Elgamal's data corresponded to the –2.9 m depth rather than –5.0 m shown here. Also, Zegal and Elgamal processed the acceleration records with a low pass filter to remove more of the high frequency response. As a result their hysteresis loops are somewhat smoother than those shown in Figure 9. The most significant difference, however, lies in the magnitudes of computed strains. Zeghal and Elgamal approximated strains using a linear interpolation of displacements. As a result their strain data has no dependence on depth, unlike the data generated here for either the homogeneous or the layered analysis. In particular, the layered analysis used here suggests significantly greater strains than does the linear analysis of Zeghal and Elgamal (1994).

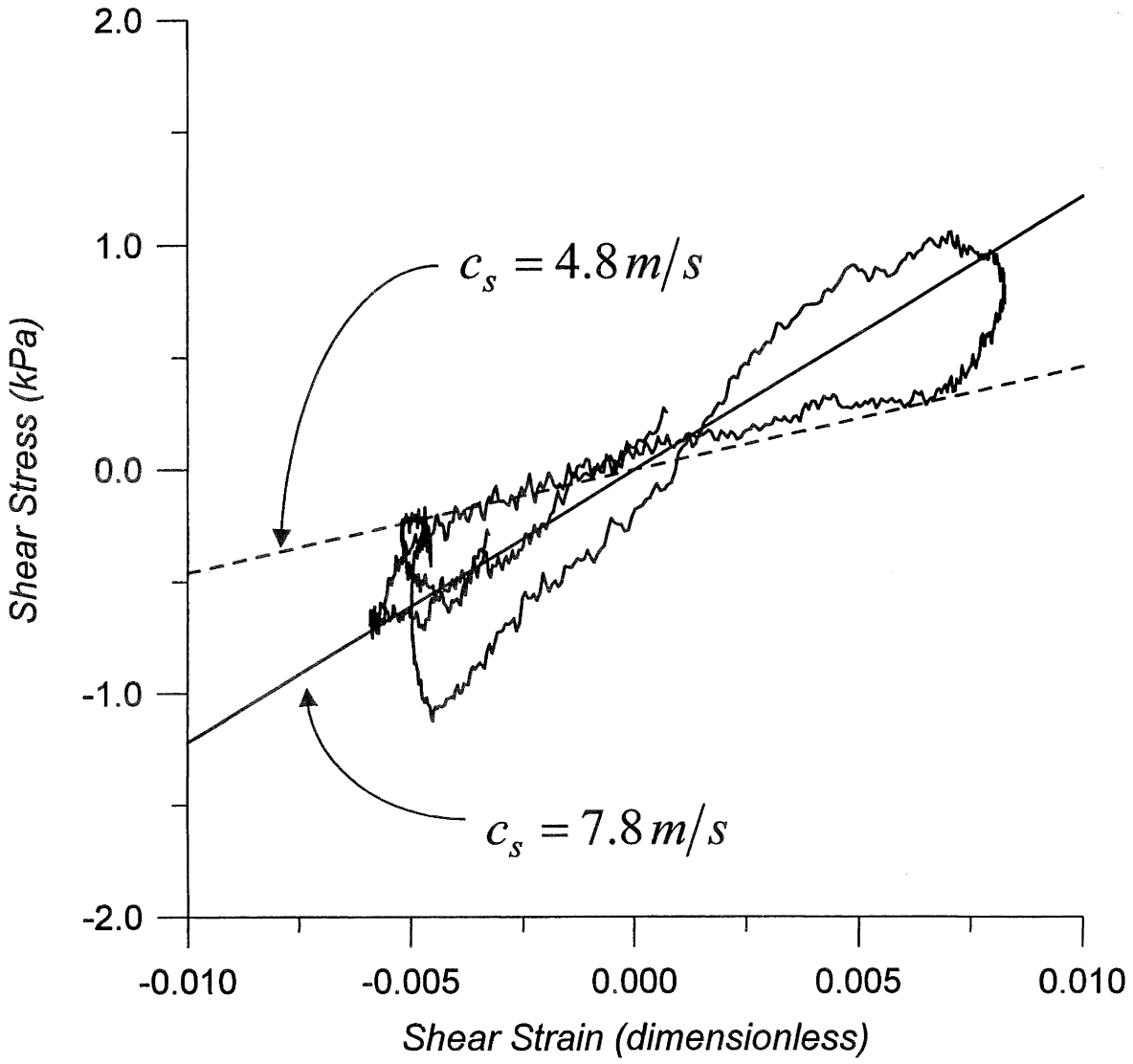

Figure 10. A small portion of the 60 to 90 second stress-strain response from Figure 9. . The straight lines represent shear moduli for the two shear wave velocities shown.

Finally, we can consider the computed value of shear strain at the onset of pore pressure rise. This can be compared with the theoretical threshold strain proposed by Dobry, *et al.* (1979,1982). The analysis proposed by Dobry together with his co-workers was based on the theory of elastic contact developed by Mindlin and Deresiewicz (1953). They investigated the behaviour of a simple packing of uniform elastic spherical particles subjected to normal and shear tractions. The normal force creates a flat circular contact between adjacent particles. If the normal force is held constant while the shear force is increased gradually, it is found that the interparticle contacts begin to yield. For moderate shear forces the yielding occurs on an annular ring surrounding a circular segment that remains elastic. If the shear force becomes sufficiently large, the entire contact area yields and gross slip may occur between particles. Dobry, *et al.*, conjectured that it was at this point that gross particle rearrangement could commence, and hence pore pressure begin to rise. According to the analysis of Mindlin and Deresiewicz (1953), the value of shear strain for which complete slip occurs may be written

$$\gamma_t = \left(\frac{3\sigma}{2G}\right)^{\frac{2}{3}} \frac{(2-\nu)f}{(1-\nu)^{1/3}} \qquad (2)$$

Here σ represents the effective stress supported by the particle skeleton, while G and V are the shear modulus and Poisson ratio for the solid particles. Also, f denotes the coefficient of friction for the interparticle contact, the so-called intrinsic friction. Typical values for G and V for soil forming minerals are 30 GPa and 0.3. A realistic value for f might be 0.5. Thus, as a general approximation, equation (2) suggests the threshold strain should be roughly

$$\gamma_t = \left(13\times10^{-6}\right)\sigma^{\frac{2}{3}} \qquad (3)$$

where σ is in kPa. The range of values for σ in the silty sand layer at Wildlife is roughly 35 to 75 kPa. Thus one might expect threshold strains ranging from about $1\text{x}10^{-4}$ in the upper parts of the layer, to $2.5\text{x}10^{-4}$ near the bottom of the layer.

We can begin to investigate the threshold strain at Wildlife by considering the Elmore Ranch earthquake. No pore pressure rise was recorded for this earthquake, hence it should provide a lower bound for the threshold strain. Typical strain time histories calculated at the –6.6 m depth using the homogeneous model of Davis and Berrill (1998) are shown in Figure 11. For this depth a peak strain of $-6.9\text{x}10^{-4}$ occurs in the East-West record at 6.695 seconds. The North-South and East-West records are nearly out of phase at this time and there would have been little contribution to the overall shear strain from the North-South motion. The computed strain magnitude is somewhat larger than the greatest threshold strain given by equation (3) but the two numbers are of the same order. Near the top of the silty sand layer, at depth –2.9 m the peak strain was $-3.9\text{x}10^{-4}$.

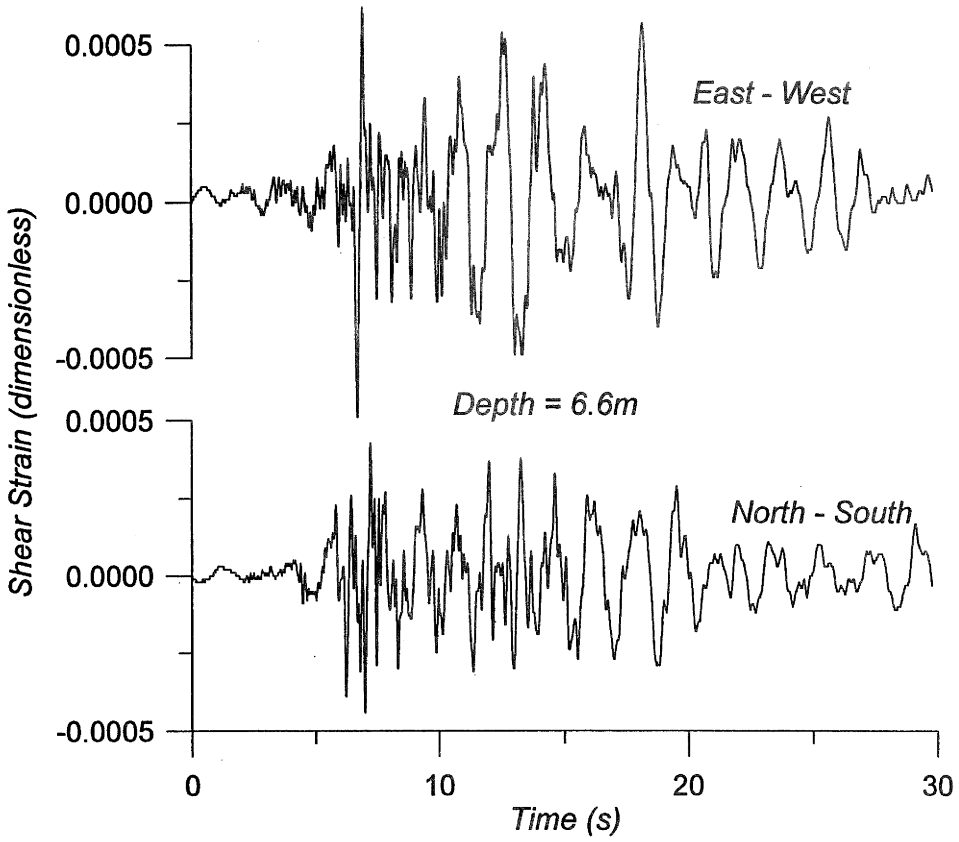

Figure 11. Synthesized shear strains from the Elmore Ranch earthquake calculated at –6.6 m depth.

Next we consider the Superstition Hills earthquake. The measured pore pressure behaviour will be discussed in detail in the following section. For the time being we only need to know how the pore pressures began to increase early in the record. Figure 12 shows the response for the initial 20 seconds of the record. All four pore pressure transducers that were operational for the Superstition Hills earthquake are shown. The records are marked *P1, P2, P3,* and *P5* corresponding to the transducer designations used by the USGS at Wildlife. The depth of placement for each transducer is shown in Table 1.

Table 1. Depths for pore pressure measurement

Designation	Depth (m)
P1	-5.0
P2	-3.0
P3	-6.6
P5	-2.9

Recalling that the silty sand layer commenced at –2.5 m, we see that *P2* and *P5* were both located near the top of the layer. The other two operational transducers were deeper with *P3* lying within 0.4 m from the bottom of the layer. Figure 13 shows the initial 20 seconds from the four pore pressure records. The *P1* and *P3* records appear more noisy than do *P2* and *P5*, and the *P3* record begins rising directly from time zero. The original investigators, Holzer, et al. (1989) and Youd and Holzer (1994), suggest that no significant piezometer response occurred prior to the peak ground acceleration at about 13.6 seconds. The vertical dashed lined on Figure 11 corresponds to this time. It appears that all the peizometers except *P2* showed some change prior to 13.6s, but Holzer, et al. (1989), attribute these changes to electronic drift.

Figure 13 shows the computed strain histories at depth –6.6 m using the layered analysis. The initial 14 seconds of the motion are shown. Evidently strains occurred at this depth that were significantly greater than the threshold strain at times before 13.6 seconds. The greatest computed strain at this depth prior to 13.6 second was –0.00158 in the East-West record at 13 seconds. At the –2.9 m depth the corresponding value was 0.00089. The peak acceleration occurred at 13.6 seconds and is clearly visible on the North-South strain history where a strain magnitude of -0.00281 occurs. The computed strains do not appear to support the calculated value of threshold strain suggested by equation (3). Perhaps this is not surprising given the idealised nature of the Mindlin- Deresiewicz analysis. Nevertheless, the *concept* of a threshold strain clearly is supported by the data.

PORE PRESSURE INCREASE AND DISSIPATED ENERGY

Finally we will attempt to model the measured pore pressure rise using a relationship between pore pressure and dissipated energy density. Nemat-Nasser and Shokooh (1979) initially proposed the pore pressure - dissipated energy relationship. They noted that in a dry granular mass, cyclic loading results in grain rearrangement and volumetric compression causing energy to be dissipated throughout the soil volume. For a saturated soil in undrained conditions, the particles are prevented from rearranging into a more dense configuration by the pore fluid. Nemat-Nasser and Shokooh postulated that the energy dissipation which resulted in volumetric strain for the dry soil should therefore result in pore pressure increase in the saturated soil. Their idea has since been investigated by a number of researchers [Davis and Berrill (1982), Simcock, *et al.* (1983), Berrill and Davis (1985), Law, *et al.* (1990), Figueroa, *et al.* (1994), Trifunaic (1995), Green, *et al.* (2000)]. Kayen and Mitchell (1997) have published a similar analysis employing Arias intensity rather than dissipated energy density. In several of these publications, comparisons between pore pressure increase and dissipated energy density measured directly in laboratory cyclic loading tests (both triaxial and torsional shear tests) were displayed. Most recently, Davis and Berrill (1999) have presented similar comparisons based on field data acquired at two instrumented sites in Japan and Taiwan. All of the research to date appears to confirm the hypothesis of a well-defined relationship between pore pressure rise and dissipated energy density.

Some researchers have assumed a simple linear relationship of the form:

$$p = \alpha D \tag{4}$$

Here p denotes pore pressure increase, D is the dissipated energy density or dissipated energy per unit volume, and α is a dimensionless constant. Generally values of α in the range 50 to 80 have been suggested by laboratory data. While equation (4) has the benefit of simplicity, it is inadequate for situations where complete liquefaction is imminent. If p approaches the value of the initial effective stress σ, then one would expect the rate of increase in p to fall off. This has led some investigators to propose a slightly more complex relationship:

$$p = \alpha D^{\beta} \tag{5}$$

This equation permits p to increase more slowly for greater values of D, but, in comparison with (4), suffers from two drawbacks: the requirement for two material parameters and loss of dimensional homogeneity. Dimensional homogeneity may be easily restored by replacing p and D in (5) with appropriately normalised variables, for example p divided by the initial static pore pressure and D divided by the initial overburden stress. The requirement for two material parameters remains a significant drawback however.

Clearly equation (4) is not adequate for the purpose of modeling the Wildlife pore pressure response since complete liquefaction did occur. While equation (5) can provide more realistic response, the requirement for two parameters is unattractive. We will propose an alternative relationship between p and D. Let

$$\dot{p} = \lambda \dot{D} \tag{6}$$

where

$$\lambda = \lambda(p) = \alpha\left(\frac{\sigma - p}{\sigma}\right) \tag{7}$$

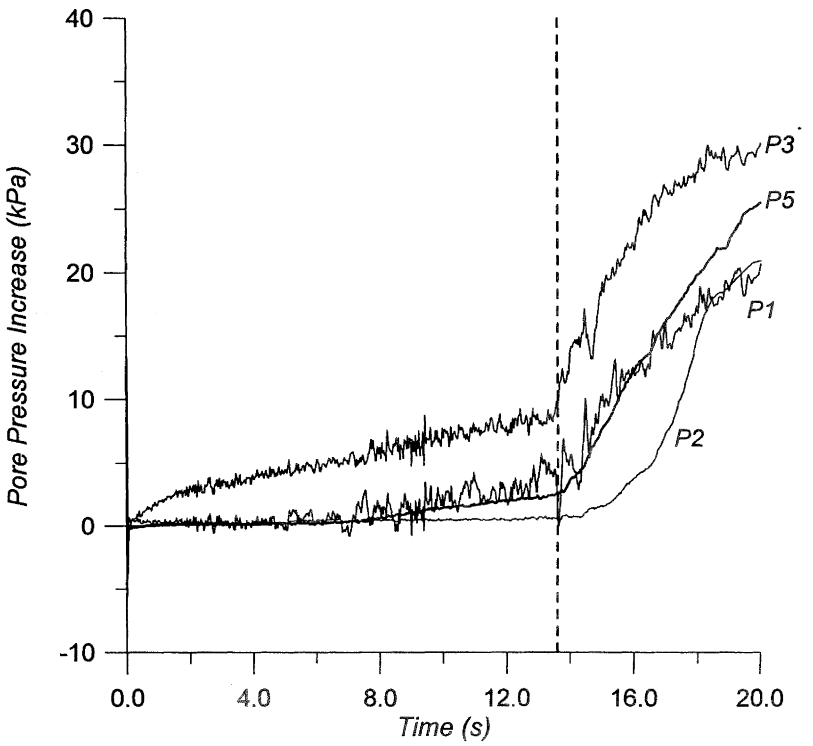

Figure 12. Initial measured pore pressure response from Superstition Hills earthquake.

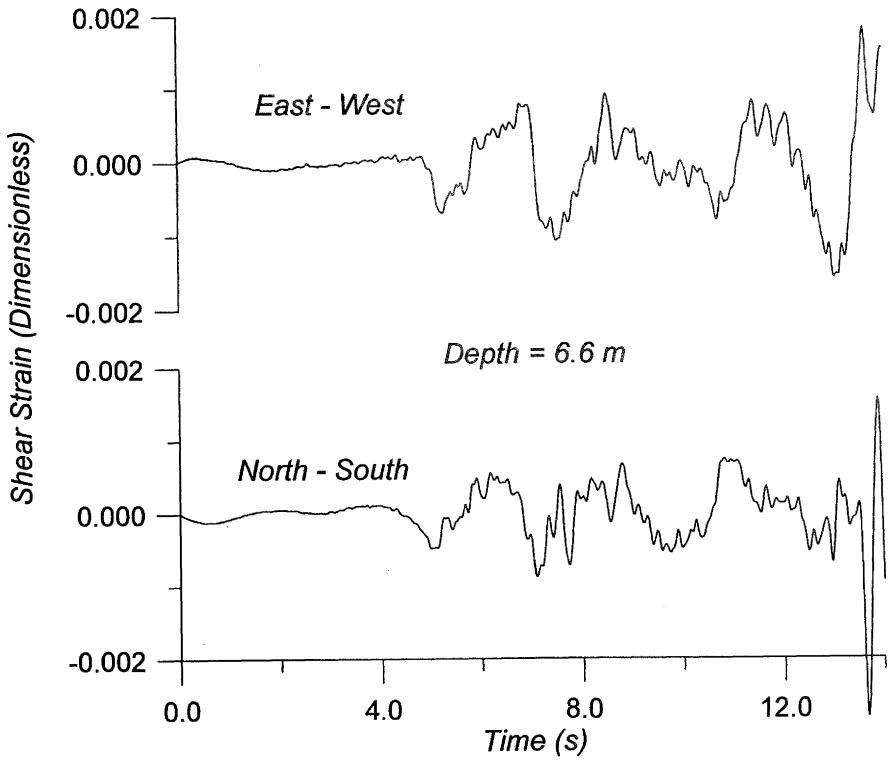

Figure 13. Synthesized shear strains from early in the Superstition Hills earthquake calculated at –6.6 m depth.

Here the superposed dot implies the time derivative, σ is the initial value of effective stress at the depth of interest, and α is the same as in equation (4). We see from equations (6) and (7) that the pore pressure response for small values of D will be the same as that for equation (4). If the pore pressure increase approaches the value of σ however, the rate of increase will slow and approach zero. Integrating equation (6) gives

$$p = \sigma\left(1 - \exp\left(\frac{-\alpha D}{\sigma}\right)\right) \tag{8}$$

Like equation (5), this model has two parameters; however, one is the initial effective stress, a quantity that presumably can be easily determined. The second parameter α is identical to that in equation (4) and might be expected to lie in range 50 to 80.

It is a simple matter to integrate the synthesized stress-strain curves discussed in the preceding section to estimate the time history of dissipated energy density D at any depth of interest in the soil profile. Letting τ denote the shear stress and $\dot{\gamma}$ the strain rate, we have

$$D = D(t) = \int_0^t \tau\dot{\gamma}\, dt \tag{9}$$

This calculation has been carried out using the synthesized shear stress and strain values for each of the depths where piezometers were placed. Both the North-South and the East-West records were used, the total dissipated energy being their sum. The resulting value for D was then used with equation (8) to synthesize the pore pressure increase at each of the piezometer depths for both of the earthquakes: Elmore Ranch and Superstition Hills. The Elmore Ranch calculation produced a maximum pore pressure increase of roughly 1.3 kPa based on a value for α in equation (8) of 200. This very small increase is consistent with the absence on any measurable pore pressure rise by the field instrumentation. The Superstition Hills calculation produced more interesting results and they are summarised below.

Figure 14 shows the results of the pore pressure predictions for the Superstition Hills event compared with the measured data. The heavy lines represent calculated pore pressure rises based on equations (8) and (9). The lighter solid lines represent measured data. Data for all four piezometers that were operational during the earthquake are shown. The value of α in equation (8) used for the calculation was 200. This is greater than the value of 50 to 80 expected. Its significance will be discussed below. It is immediately evident from Figure 14 that the *P2* and *P5* records are fairly well represented by the calculated pore pressure response. The measured data for *P5* are slightly anomalous to begin with since the peak measured pore pressure rise exceeded the initial effective stress by roughly 20 percent (Youd and Holzer, 1994). Clearly, the format of equation (8) will not permit the calculated value of p to exceed the initial effective stress. The response of *P2*, at nearly the same depth, lies closer to the expected value of the initial effective stress. At greater depths the modeled pore pressure increase occurs more quickly. This results from greater dissipation of energy deeper in the layer caused by greater stresses and strains. This comment can be generalised. The free surface boundary condition ensures no dissipated energy can occur at zero depth. In general then, for a homogeneous material, dissipated energy density must increase with increasing depth. In a layered soil profile the generalisation may break down; but, as a rule of thumb, the pore pressure-dissipated energy model suggests liquefaction should commence deeper in a soil layer sooner than at shallower locations. The measured response for *P1* and *P3* both show much slower increases. Both data appear to be converging on the calculated p values, but the rate of pore pressure rise appears quite slow.

As noted above, the value of α used to generate the theoretical curves in Figure 14 is greater than might be expected from results of laboratory tests. Smaller values of α can be used but the agreement with the experimental data breaks down fairly rapidly if α is decreased. The high value for α suggested here may be due to the nature of the Wildlife soil. Whereas most laboratory data have been generated using clean sands, the soil at Wildlife is described by Youd and Holzer as a thinly cross-bedded silty sand. The fines content (< 0.075 mm) is given by Holzer *et al.* (1989) as about 33 percent. In the usual context of liquefaction studies, the large silt content at Wildlife is somewhat unusual. Ishihara (1996) notes that silty sands generally have a higher void ratio and tend to be more contractive than clean sands. Also, Green, *et al.* (2000), relate that their parameter PEC, which is inversely related to our α, takes on smaller values for finer grained soils. These remarks would suggest the potential for a higher value for α.

An additional reason for increased α may stem from the interbedded nature of the site soils. Thin layers of silt may act to impede drainage and hence slow the dissipation of excess pore pressures from surrounding sand layers. This would result in a stronger pore pressure generation mechanism than might otherwise be the case. Yet another possible explanation may lie in the possible existence of significant surface wave effects. The calculated pore pressures shown here assume vertically propagating shear waves are the only source of energy. In fact, some of the energy introduced to the site may be in the form of surface waves. This could easily account for greater pore pressures and hence an apparently greater influence for the vertical waves than is actually the case.

Finally, we will briefly consider the early response of the measured and computed pore pressures. Figure 15 shows the initial 14 seconds from Figure 14 with an expanded pore pressure scale. Evidently the calculated pore pressures (heavy line) indicate a small initial rise well before the peak acceleration at 13.6 seconds. The predicted pore pressures all jump to some degree at roughly 7 seconds. The piezometer *P2* showed no indication of a rise at this time, but both *P1* and *P5* do suggest a small change in the pore pressure response. It is difficult to draw any conclusion from the *P3* record, although the measured and predicted pore pressures look remarkably similar following 7 seconds. If we investigate the acceleration records, a significant acceleration spike was recorded in the East-West direction at about this time. Its magnitude was roughly -123 cm/s^2. Prior to that point, no acceleration exceeding 100 cm/s^2 had been recorded in either direction, although the Elmore Ranch event 12 hours earlier had a peak acceleration of nearly the same value. The computed strain histories in Figure 13 do not suggest a major change occurred at 7 seconds, but a local strain maximum

does occur at roughly that time on both North-South and East-West records. The computed strains are on the order of $1x10^{-3}$, still considerably greater than the threshold strain of Dobry, *et al.* (1982).

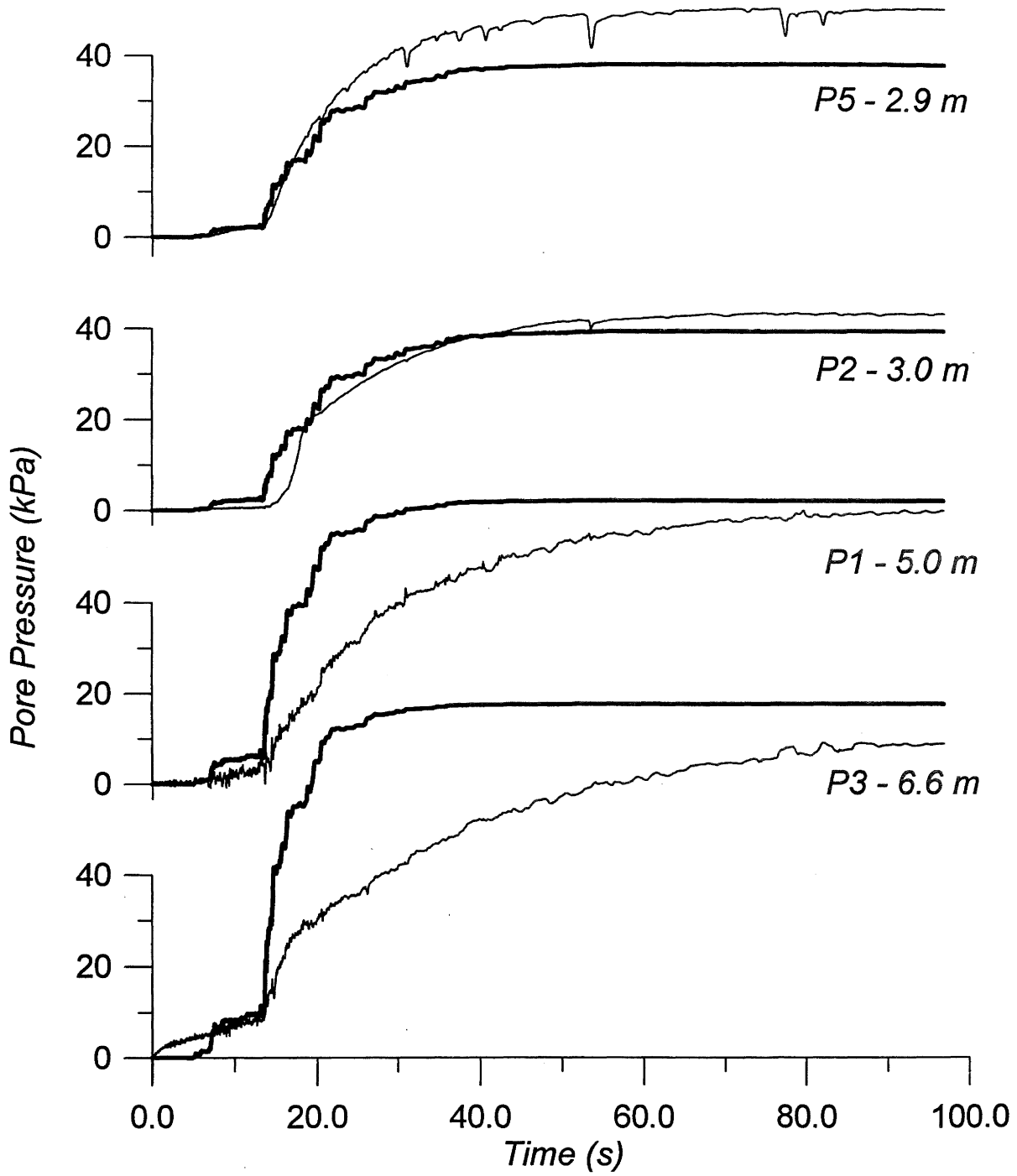

Figure 14. Pore pressure increase from Superstition Hills earthquake. Heavy lines are calculated values. Light lines are measured values.

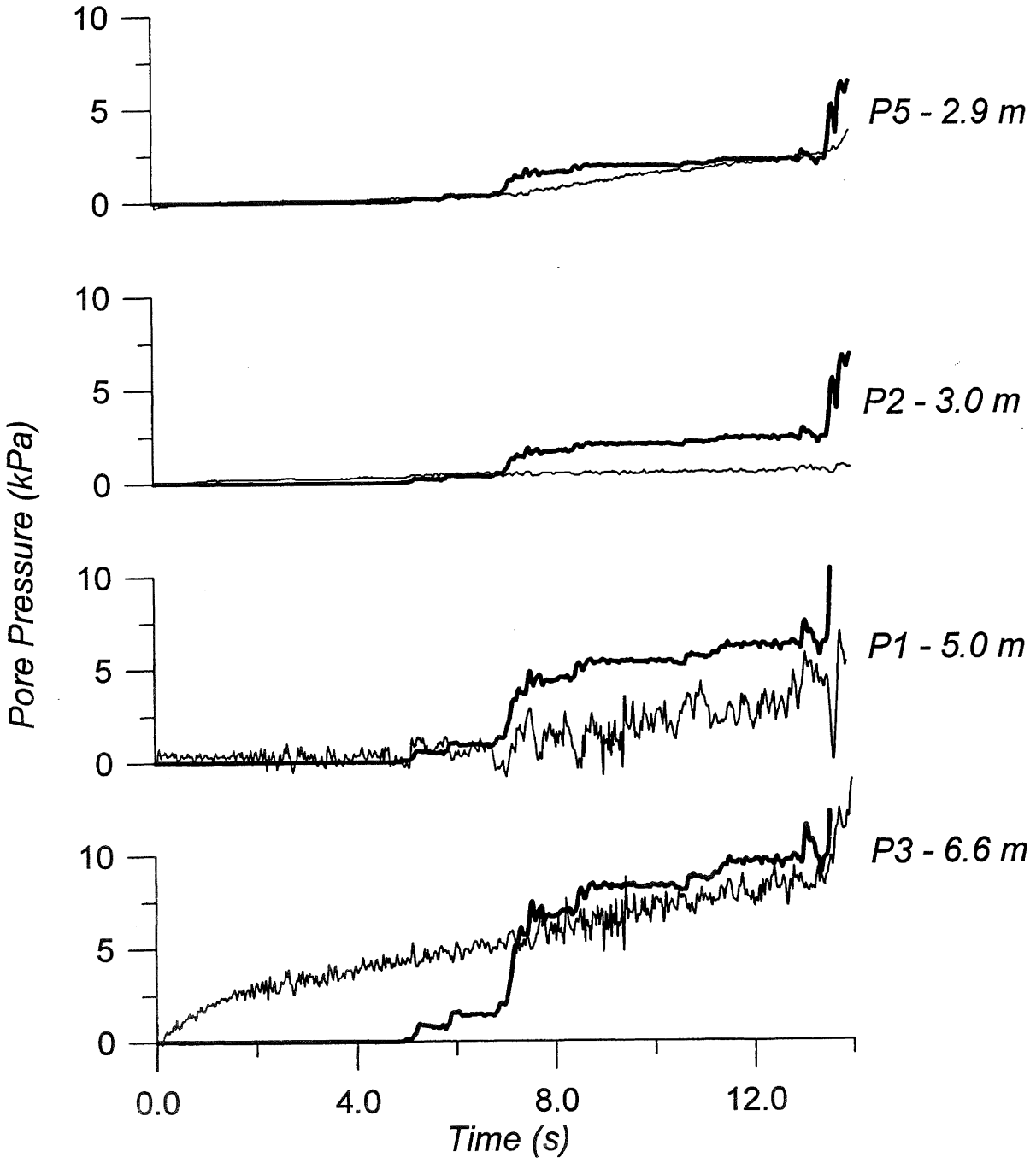

Figure 15. Early pore pressure response from Superstition Hills earthquake. Heavy lines are calculated values. Light lines are measured values.

CONCLUSIONS

It seems clear the Wildlife records represent both a valuable resource and a significant challenge. They have been the subject of investigation by a number of researchers, but remain, to some extent at least, an enigma. In this paper we have attempted to shed some additional light on both soil softening and pore pressure response during the Superstition Hills earthquake. We have synthesized the pore pressure response using a pore pressure-dissipated energy relationship. Reasonably good agreement is found in the case of two of the measured pore pressure records, but it is necessary to use a value for the model parameter α that is greater than values suggested from laboratory tests on other soils. Measured pore pressures for the two piezometers located deeper in the liquefying layer appear to rise more slowly than the predicted values would indicate. In general, the pore pressure-dissipated energy relationship suggests more rapid pore pressure development will occur at greater depths.

We have attempted to synthesize stress-strain response within the liquefying layer. This calculation was based on acceleration and displacement records from the ground surface at –7.5 m depths. We have taken into account the

layered soil profile at Wildlife with the result that calculated strains are somewhat larger than previously indicated, especially later in the record. We have compared the computed strain values with the theoretical threshold strain proposed by Dobry, *et al.* (1982). It would appear the actual strains prior to the onset of pore pressure increase were significantly larger than Dobry's threshold value. Nevertheless, both the measured and the computed pore pressure response strongly support the concept of some type of threshold being active at Wildlife. The pore pressure increase began abruptly and simultaneously in all four piezometers at the time the peak ground acceleration occurred.

The possible importance of surface wave effects has been emphasised in regard to both the interpretation of softening and the prediction of pore pressure based on downhole acceleration data. While the approximation of site response using one-dimensional, vertically propagating shear waves is clearly a great convenience, three-dimensional effects may play a significant role. Unfortunately, simple downhole accelerometer arrays are not sufficient to indicate the presence of surface waves. Full three-dimensional arrays will be required to make definitive decisions regarding the importance or otherwise of surface waves.

ACKNOWLEDGEMENT

This study was funded by the New Zealand Earthquake Commission Research Foundation under projects numbered 99/340 and 99/345. We are grateful to Professor Ralph Archuleta of the University of California at Santa Barbara for discussions that led to the work reported here and for providing the Wildlife data for our use.

REFERENCES

Archuleta, R.J. (1998) "Direct observation of nonlinearity in accelerograms." *Proc. 2nd Int. Symp. Effects of Surface Geology on Seismic Motion*, eds. K. Irikura, K. Kudo, H. Okada and T. Sasatani, A.Abalkema, pp.787-792.

Berrill, R.O. and Davis, R.O. (1985) "Energy dissipation and seismic liquefaction in sands: Revised model." *Soils and Foundations*, **25**, no. 2, 106-118.

Davis, R.O., and Berrill, J.B. (1982) "Energy dissipation and seismic liquefaction in sands." *Earthquake Engg. Structural Dynamics*, **10**, 59-68.

Davis, R.O. and Berrill, J.B. (1998) "Rational approximation of stress and strain based on downhole acceleration measurements" *Int. J. Numer. Anal. Meth. Geomech.*, **22**, 603-619.

Davis, R.O. (2000) "Estimation of soil shear modulus softening during strong ground shaking using ground surface and downhole acceleration recordings." *Earthquake Engg. Structural Dynamics*, **29**, 359-376..

Davis, R.O. and Berrill, J.B. (1999) "Correlation of pore pressure and dissipated energy in earthquakes – Field verification." *J. Geotech. and Geoenviron. Engg.*, ASCE, submitted for publication.

Dobry, R. and Swiger, W.F. (1979) "Threshold strain and cyclic behavior of cohesionless soils." *Proc. ASCE Engineering Mech. Speciality Conf (3rd)*, University of Texas, Austin, pp 521-525.

Dobry, R., Ladd, R.S., Yokel, F.Y., Chung, R.M., and Powell, D. (1982) "Prediction of pore water pressure buildup and liquefaction of sands during earthquakes by the cyclic strain method." *NBS Building Science Series 138*, National Bureau of Standards, 150pp.

Figueroa, J.L., Saada, A.S., Liang, L., and Dahisaria, M.N. (1994) "Evaluation of soil liquefaction by energy principles." *Jour. Geotech. Engg.*, ASCE, **120**, 1554-1569.

Green, R.A., Mitchell, J.K., and Polito, C.P. (2000). "An energy based excess pore pressure generation model for cohesionless soils." *Proc. John Booker Memorial Symposium*, Sydney, Balkema, in press.

Holzer, T.L., Youd, T.L., and Hanks, T.C. (1989). "Dynamics of liquefaction during the Superstition Hills Earthquake (M+6.5) of November 24, 1987." *Science*, **244**, April 7, 56-59.

Hushmand, B., Scott, R.F., and Crouse, C.B. (1992). "In-place calibration of USGS transducers at Wildlife liquefaction site, California, USA." *Proc. 10th World Conf. On Earthquake Engg.*, A.A.Balkema, Rotterdam, 1263-1268.

Ishihara, K. (1996). *Soil Behaviour in Engineering Geotechnics*, Oxford University Press, 350 pp.

Kayen, R.E. and Mitchell, J.K. (1997). "Assessment of liquefaction potential during earthquakes by Arias intensity." *Jour. Geotech. Geoenviron. Engg.*, ASCE, **123**, pp.1162-1174.

Law, K.T., Cao, Y.L., and He, G.N. (1990) "An energy approach for assessing seismic liquefaction potential." *Canadian Geotech. Jour.*, **27**, 320-329.

Mindlin, R.D. and Deresiewicz, H. (1953) "Elastic spheres in contact under varying oblique forces." *Jour. Appl. Mech.* ASME, pp.203-208.

Nemat-Nasser, S., and Shokooh, A.S. (1979) "A unified approach to densification and liquefaction of cohesionless sand in cyclic shearing." *Canadian Geotech. Jour.*, **16**, 659-678.

Simcock, K.J., Davis, R.O., Berrill, J.B. and Mullenger, G. (1983) "Cyclic Triaxial Tests with Continuous Measurement of Dissipated Energy." *Geotechnical Testing J.*, **6**, pp. 35-39.

Trifunac, M. (1995) "Empirical criteria for liquefaction in sands via standard penetration tests and seismic wave energy." *Soil Dynamics Earthquake Engg.*, **14**, 419-426.

Youd, T.L. and Holzer, T.L. (1994) "Piezometer performance at Wildlife Liquefaction Site, California." *Jour. Geotech. Engg.*, ASCE, **120**, pp.975-995.

Zeghal, M., and Elgamal, A.W. (1994). "Analysis of site using earthquake records." *J. Geotech. Engg.*, ASCE, **120**, 996-1017.